EPJ manuscript No.
(will be inserted by the editor)

arXiv:physics/0612224v1 [physics.bio-ph] 22 Dec 2006

Bubbles and denaturation in DNA

Titus S. van Erp[1] e-mail: Titus.VanErp@biw.kuleuven.be, Santiago Cuesta-López[2,3], and Michel Peyrard[2]

[1] Centre for Surface Chemistry and Catalysis, Catholic University of Leuven, Kasteelpark Arenberg 23, 3001 Leuven, Belgium
[2] Laboratoire de Physique, Ecole Normale Supérieure de Lyon, 46 allée d'Italie, 69364 Lyon Cedex 07, France
[3] Dept. Condensed Matter Physics and Institut of Biocomputation and Complex Systems. University of Zaragoza, c/ Pedro Cerbuna s/n 50009 Spain

the date of receipt and acceptance should be inserted later

Abstract. The local opening of DNA is an intriguing phenomenon from a statistical physics point of view, but is also essential for its biological function. For instance, the transcription and replication of our genetic code can not take place without the unwinding of the DNA double helix. Although these biological processes are driven by proteins, there might well be a relation between these biological openings and the spontaneous bubble formation due to thermal fluctuations. Mesoscopic models, like the Peyrard-Bishop-Dauxois model, have fairly accurately reproduced some experimental denaturation curves and the sharp phase transition in the thermodynamic limit. It is, hence, tempting to see whether these models could be used to predict the biological activity of DNA. In a previous study, we introduced a method that allows to obtain very accurate results on this subject, which showed that some previous claims in this direction, based on molecular dynamics studies, were premature. This could either imply that the present PBD should be improved or that biological activity can only be predicted in a more complex frame work that involves interactions with proteins and super helical stresses. In this article, we give detailed description of the statistical method introduced before. Moreover, for several DNA sequences, we give a thorough analysis of the bubble-statistics as function of position and bubble size and the so-called l-denaturation curves that can be measured experimentally. These show that some important experimental observations are missing in the present model. We discuss how the present model could be improved.

PACS. 87.15.Aa Theory and modeling; computer simulation – 87.15.He Dynamics and conformational changes – 05.10.-a Computational methods in statistical physics and nonlinear dynamics

1 Introduction

The process of DNA denaturation has intrigued both biologists as statistical physicists. Large openings, the so-called DNA bubbles are supposed to allow the formation of some specific DNA structures, such as the T-loop that stabilizes the end of the chromosomes. The opening of the DNA double helix is also a mandatory step for the transcription and the replication of the genetic code. In addition, the bonds between bases on opposite strands can break due to thermal fluctuations which can occur even at room or physiological temperatures. These thermally induced DNA bubbles can be several base-pairs long and tend to increase at higher temperatures, which eventually results in the complete denaturation or the melting of DNA. An intriguing question we could ask ourselves is how the formation of bubbles depend on the base-pair specific sequence and how thermally induced bubbles relate to biophysical DNA unwinding mechanisms that are involved in the transcription and replication. Although these biological processes are driven by proteins, the intrinsic fluctuations of DNA itself might play an important role. Hence, one could even question whether biological active sites could be predicted by thermally induced bubbles in absence of any proteins [1,2,3].

Experimentally, the thermally induced denaturation can be monitored as the breaking of the base-pairs is accompanied with a large increase of UV absorbance near 260 nm. In fact, the UV absorbance measures the reduction of base-pairing and -stacking when the DNA molecule denaturates. Using this technique, it was found that large synthetical fabricated homopolymers denaturate suddenly within a very small temperature interval [4]. This indicates that the process resembles a true first order phase transition. On the other hand, natural heterogeneous DNA polymers denaturate in multiple steps and the shape of this denaturation curve is highly sensitive to the sequence [5]. It is known that this process is not only determined by the fraction of strong (GC) or weak (AT) bonds. The sequence specific order is also important. Specific sequences can reveal a high opening rate despite a high fraction of GC base-pairs [6]. Besides the already mentioned UV absorbance experiments, many ingenious techniques have been devised to study the denaturation process and the statistical and dynamical properties of DNA bubbles in general. For instance, Raman vibrational spectroscopy [7,8], neutron scattering [9], fluorescent correlated spectroscopy [10] and S1-nuclease cleavage [1] have recently put forward as promising experimental tools to gain insight in the complex mechanism of DNA denaturation.

In general, despite this significant progress, the experimental techniques reveal only indirect information. Hence, complementary computational and theoretical studies are often a requisite to complete the interpretation of experimental data. This is, however, difficult due to the astronomical large number of atoms that are needed to describe solvated DNA. Besides the number of atoms of DNA itself, a sufficiently large number of water molecules and counter ions should be included. Any full-atom approach is henceforth limited to very short DNA sequences and, for the longest sequences that can be studied, meaningful bubble statistics cannot be obtained. This has created need for mesoscopic theoretical models that allow to study long DNA sequences of hundreds or even thousands of base-pairs [11,12,13,14,15,16]. While most of these models try to mimic the system by an Ising-like model, the Peyrard-Bishop-Dauxois model [15,16] (PBD) relies on a continuous approach using an effective force-field as function of the base-pair separation. Although more complicated than the Ising type models, the PBD model has the advantage that it can describe the DNA sequence in a more detailed manner than just a simple array of open and closed states and it allows to study dynamics as well. An important essence of the PBD model is the nonlinear stacking interaction which reproduces the experimentally measured sharp phase transition of long homopolymers [16]. Moreover, the model, parameterized for heterogeneous DNA chains, has given accurate results for denaturation curves of short heterogeneous DNA sequences [17]. Although the PBD model is a very strong simplification of the actual DNA molecule in solution, the qualitative and even quantitative agreement with numerous experimental findings have given confidence to this model and to its theoretical results for which yet no direct experimental information is available.

It were these findings that inspired Choi *et al.* [1,2] to compare the signal of S1 nuclease cleavage experiments with the formation of bubbles of a certain size obtained from molecular dynamics (MD) simulations of PBD model. The detection of bubbles at a certain size requires the identification of configurations that contain series of consecutive open base-pairs which is very difficult to accomplish experimentally. Still, as argued in [1], the S1 nuclease enzymes can selectively cleave the large temporary openings while leaving the smaller openings intact, hindered by their own physical size. The amount of cleavages at certain positions in the DNA chain results in a signal that becomes visible after a certain time of incubation (about 45 min. [1]). The obtained S1 nuclease signal showed a remarkable correspondence with the calculated probability profile for bubbles containing ten or more base-pairs from the MD simulations of the PBD model [1]. Moreover, both experimental and theoretical graphs showed clear dominant peaks around the Transcription Start Site (TSS) where the biological transcription is initiated. A similar result had been reported by Benham *et al.* [18,19,20,21,22] who also found a connection between bubble formation and regulatory loci using a theoretical model. However, there are two crucial differences between the work of Benham *et al.* and Choi *et al.* First, the methodology of Benham *et al.* is specified to detect very large openings upto 100 base-pairs in kilobase sequences, while the work of Choi *et al.* investigates much smaller openings ~ 10 in sequences of the order ~ 100 base-pairs. The second and most important difference is that work of Benham studies the bubbles *in vivo* which includes torsional effects that are generated by other molecules. The apparent evidence of Choi [1] suggested that spontaneous bubbles *in vitro* already bear the signature of biological activity. A remarkable result that was summarized by the statement: *DNA directs its own transcription* [1].

Unfortunately, this statement had to be reconsidered due to more accurate results by us [3] using a direct integration method that is orders-of-magnitude faster than MD. An important difficulty with MD or Monte Carlo is that large bubbles appear only seldom so that the statistical significance can be questioned even for very long simulation periods. Our accurate results did not support the previously found results at some crucial points. As in [1], they indicated that bubbles might appear more easily in the biological active sites due to its higher content of AT as compared to a random sequence. However, contrary to [1], the most dominant peak did not appear at the TSS for the sequences under study nor did the promoter sequences have a much higher opening profile as compared to biologically inactive sequences. Hence, the statistical information on bubbles obtained by the PBD model was found to be insufficient to make very accurate predictions on transcription start sites or to discriminate between promoter sequences and biologically inactive sequences as was suggested before [1,2]. This leaves open the following possibilities: (i) either the transcription sites cannot be predicted by the information on thermally induced bubbles alone but require more complex interactions including, for instance, superhelical stress, or (ii) the bubble hypothesis of Choi *et al.* still holds, as suggested by the S1 nuclease experiments, but a more accurate theoretical model is needed to support these findings.

The main subject of this article is to give a detailed description of the direct integration method introduced in [3] and to show some examples of the calculated bubble statistics for some biologically active and inactive sequences. We will also investigate the validity of the PBD model by applying this method to calculate quantities that allow a more direct comparison with experiments. This article is organized as follows: we will first give a short introduction to the PBD model in Sec. 2, followed by a theoretical discussion on what we will call the double stranded DNA ensemble (dsDNAE) in Sec. 3. The latter is needed to give meaningful results when applying the PBD model to finite chains. Then, in Sec. 4, we give some important definitions concerning the bubble statistics of DNA expressed in microscopic terms such that it can be calculated by computer experiments. In

Sec. 5 we introduce the direct integration method including all the technicalities involved. This derivation results in an algorithm that implies a repetitive numerical integration scheme using a Newton-Cotes rule. The efficiency of several Newton-Cotes schemes, such as rectangular, trapezoidal, Simpson's $\frac{1}{3}$-rule, Boole's rule, and 11-point Newton-Cotes rule, are examined and compared in Appendix A. In Sec. 6 we show some numerical results of the bubble probability profiles of a biologically active promoter sequence and two artificial Fibonacci sequences. We confirm the previous findings: there is no enhanced opening at transcription start sites or at promoter sequences in comparison to biologically inactive sites and sequences that have a similar (local) AT content. Then, in Sec. 7 we investigate the validity of the PBD model using the direct integration method to calculate l-denaturation curves which can be measured experimentally by the recently introduced quenching technique[23,24,25]. These results clearly indicate that some essential ingredients are missing in the present PBD model. This implies that the PBD model should be improved and that the bubble hypothesis of Choi *et al.* could still hold when an 'ideal theoretical model' is considered. In Sec. 8, we end with a general discussion and make some suggestion that could lead to an improved theoretical model.

2 The PBD model

The PBD model reduces the myriad degrees of freedom of DNA to a one-dimensional chain of effective atom compounds describing the relative base-pair separations y_k from the ground state positions. The total potential energy U for an N base-pair DNA chain is then given by

$$U(y^N) \equiv V_1(y_1) + \sum_{k=2}^{N} V_k(y_k) + W(y_k, y_{k-1}). \qquad (1)$$

Here, $y^N \equiv \{y_k\}$ denotes the set of relative base pair positions and V_k and W are the two PBD-potential energy functions given by

$$V_k(y_k) = D_k\Big(e^{-a_k y_k} - 1\Big)^2 \qquad (2)$$
$$W(y_k, y_{k-1}) = \frac{1}{2}K\Big(1 + \rho e^{-\alpha(y_k+y_{k-1})}\Big)(y_k - y_{k-1})^2$$

The first term V_k is the on site Morse potential describing the hydrogen bond interaction between bases on opposite strands. D_k and a_k determine the depth and width of the Morse potential and are different for the weak AT and strong GC base-pair. The stacking potential W consists of a harmonic and a nonlinear term. An important reason for the success of this model lies in the ρ-term which was introduced in [16] as an improvement upon the original Peyrard-Bishop (PB) model [15]. This original PB model can be retrieved by taking $\rho = 0$. The precise analytical shape of $W(y_k, y_{k-1})$ in Eq. (2) is not crucial. What is important is that for $\rho > 0$, the effective coupling constant of the stacking interaction drops from $K' = K(1 + \rho)$ down to $K' = K$ whenever either y_k or y_{k-1} becomes significant larger than α^{-1}. It is thanks to this additional term that the observed sharp phase transition in denaturation experiments [4] can be reproduced. It is important to note the + sign in Eq. (2). This makes the stacking potential $W(y_k, y_{k-1})$ not a simple function of the relative distance $|y_k - y_{k-1}|$. It was found that, after replacing $e^{-\alpha(y_k+y_{k-1})}$ with $e^{-\alpha|y_k-y_{k-1}|}$ in Eq. (2), the denaturation transition becomes continuous again as in the original PB model [26]. However, Eq. (2) is surely not the only possible possible potential that can reproduce the sharp transition. Recently, an alternative potential $W(y_k, y_{k-1})$ was suggested in [27] which also seems to generate a sharp denaturation and only depends $|y_k - y_{k-1}|$. This shows that reproducing experimental curves alone is definitely not enough to uniquely determine the effective potentials. Interpretation of the physical mechanism that lead to the sharp denaturation transition is a prerequisite for the justification of the effective models. The discussion of this mechanism is definitely not completely settled, but the argumentation that relies in the PBD model seems very plausible, as the ρ-term mimics the effect of decreasing overlap between π electrons when one of two neighboring base move out of stack.

After modeling homogeneous DNA, Campa and Giansanti generalized the PBD model for the heterogeneous case [17,28]. The in total 7 parameters $K = 0.025$ eV/Å^2, $\rho = 2$, $\alpha = 0.35$ Å^{-1}, $D_w = 0.05$ eV, $D_s = 0.075$ eV, $a_w = 4.2$ Å^{-1}, $a_s = 6.9$ Å^{-1}, were derived by fitting to experimental denaturation curves of short heterogeneous DNA segments. The subscripts w and s refer to the type of base-pair at site k in Eq. (2). Here, D_w and a_w are used for the weak AT base-pairs and D_s and a_s are used for the strong GC base-pairs. The ratio between D_w and D_s reflects the ratio between the number of hydrogen bonds forming the AT and GC base-pair bonding. In fact, the reason to fix this ratio is not really justified as the depth of the Morse potential does not only reflect the hydrogen bond linking (which is in the order of 0.2 eV per hydrogen bond), but also the repulsive interactions of the phosphate groups and the effect of the solvent. Still, the absolute and relative magnitude of the effective weak and strong interactions seem to be more or less correct as this parameterization could reproduce the experimental denaturation curves of several short DNA sequences as tested in [17,28].

Despite these accomplishments, it is also important to realize the limitations of the model. The PBD model treats the A and T bases and the G and C bases as identical objects. The stacking interaction $W(y_k, y_{k-1})$ is also independent of the nature of the bases at site k and $k-1$. Experimental measurements [29,30,31] and theoretical calculations [32,33,34,35,36] have shown that these are rather crude approximations. Future work might aim to improve upon this.

3 The dsDNA ensemble

In this section we will assert the need of special ensemble that we will call the double stranded DNA ensemble (dsDNAE) and we will give its mathematical definition. The reason that we will not use the full NVT or NVE ensemble is because the results based on the PBD model have not much meaning in these ensembles whenever finite DNA chains are considered. The original papers using the PBD model were all performed in the thermodynamic limit of an infinite DNA chain where this problem does not appear. It is in this limit that one can show, using the transfer integral technique [37], that the uniform PBD-DNA sequence undergoes a very sharp phase transition [38] upon heating, which is first order except in a cross over region near the transition temperature that is so narrow that it is not accessible to experiments. The difficulty of finite sequences is that PBD model basically represents a single DNA chain in an infinite solution. Hence, whenever the dsDNA completely separates, the two strands are free to go to very large separations without cost of energy due to the plateau of the Morse potential. In experiments, where the amount of solvated DNA is not infinitely diluted, this effect is counterbalanced by the hybridization mechanism where two single stranded chains in solution come together and match their complementary bases. This implies that, per definition, the PBD model cannot reproduce the experimental data, which are based on finite concentrations, using equilibrium statistics in the full phase space. A confinement of the phase space is *always* necessary. These can be done hiddenly using a series of reasonable short MD [16,39,27] or Monte Carlo [40] simulations starting from a certain distribution of initial configurations. Here, the finite simulation length prohibit the boundless exploration of the completely separated states. However, this strategy will naturally generate results that depend on the choice of initial conditions and the simulation length which is not completely under control especially at temperatures near the melting transition [16,39]. Alternatively, one could restrict configuration space by adding an infinite wall such that y_k for all k cannot exceed a certain maximum value [41] or by adding a small positive slope to the plateau of the Morse potential [38]. These approaches still allow for complete denaturation and recombination of the two strands, but prevent separations of very large distances. This recombination, however, is quite artificial as the one-dimensional model does not allow for misfolding, the creation of bulge-loops [42] or the recombination with a different strand in solution. Therefore, we chose to focus to these configurations only that belong to the dsDNAE that we will introduce here. In microscopic terms, a configuration $\{y_k\}$ is called a double stranded DNA (dsDNA) molecule when $y_k < \xi$ for at least one $k \in [1 : N]$ with ξ the opening threshold definition. Similarly, a configuration is completely denaturated whenever $y_k > \xi$ for all k. All configurations assigned as dsDNA together with their corresponding Boltzmann-weight comprise the dsDNAE.

The statistical average of a certain function $A(y^N)$ in the full phase space is standardly defined as

$$\langle A \rangle \equiv \frac{\int \mathrm{d}y^N A(y^N)\varrho(y^N)}{\int \mathrm{d}y^N \varrho(y^N)} \tag{3}$$

with $\mathrm{d}y^N \equiv \mathrm{d}y_N \mathrm{d}y_{N-1} \ldots \mathrm{d}y_1$, $\varrho = e^{-\beta U}$ the probability distribution density, and $\beta = 1/k_B T$ with T the temperature and k_B the Boltzmann constant. In order to define the ensemble average in the dsDNAE we introduce following characteristic functions that indicate whether a certain base-pair is open or closed.

$$\theta_k(y_k) \equiv \theta(y_k - \xi), \qquad \bar{\theta}_k(y_k) \equiv \theta(\xi - y_k) \tag{4}$$

Here $\theta(\cdot)$ equals the Heaviside step function. θ_k equals 1 if the base-pair is open and is zero otherwise. $\bar{\theta}_k$ is the reverse. Now, the ensemble average of $A(y^N)$ in dsDNAE can be expressed as a weighted average using the weight function $\mu(y^N)$:

$$\left\langle A(y^N) \right\rangle_\mu \equiv \frac{\left\langle A(y^N)\mu \right\rangle}{\langle \mu \rangle} \tag{5}$$

with

$$\mu \equiv 1 - \prod_{k=1}^{N} \theta_k \tag{6}$$

To shorten the notation we have dropped the y_k dependencies. In Eq. (6), $\mu = 1$ except when all bases are open; then $\mu = 0$. The dsDNAE removes all difficulties concerning the unnormalizability of the full phase space equilibrium distribution. Besides the opening threshold definition ξ, it does not add any new (hidden) parameters to the PBD model as in previous examples. At temperatures sufficiently below the denaturation transition, the dsDNAE gives a good representation of the actual experimental situation where only a fraction of the DNA is in the single stranded state. It is reasonably simple to use MD in the dsDNAE using a biasing-potential, e.g. [3]

$$V^{\mathrm{bias}}(y_{\min}) = \begin{cases} (y_{\min} - \xi)^6 & \text{if } y_{\min} > \xi \\ 0 & \text{otherwise} \end{cases} \tag{7}$$
$$\text{with } y_{\min} = \mathrm{MIN}[\{y_k\}]$$

This bias yields an additional force to the system that is always zero except when the dsDNA is at the point of complete denaturation. Then it gives a strong repulsion to the last closed base to prevent the complete opening of the whole molecule. Although, MD is certainly much less efficient than the direct integration method expressed in Sec. 5, MD using the biasing force (7) can still be useful for calculating properties that do not allow the factorization necessary for the integration method or dynamical properties. At higher temperatures, the contributions of single stranded DNA, to e.g. UV absorbance, can no longer be neglected. Luckily, recent experimental techniques allow to selectively subtract the contributions of the single stranded molecules to the signal [23,24,25] such that, effectively, the dsDNA signal can be obtained. Hence, also at higher temperatures, the theoretical PBD calculations using dsDNAE can be compared with experimental results.

It is an interesting mathematical problem why the complete separation does not disturb the thermodynamic case. In fact, this can be understood invoking one-dimensional random walk theory. This reveals that, for a fixed configuration of the infinite DNA chain, one should always meet a closed base-pair when making a walk in one direction along the chain [1]. Hence, μ is always 1 for the infinite case and, thus, the infinite chain remains in the dsDNAE at all times. It is important to note that, therefore, the constraint to keep always one base-pair closed, does not destroy the phase transition. On contrary, the additional constraint allows to study thermodynamic limit using finite approximants in a much more controlled way. Fig. 1 shows the denaturation curves of finite homopolymers of increasing length. The results was obtained by the direct

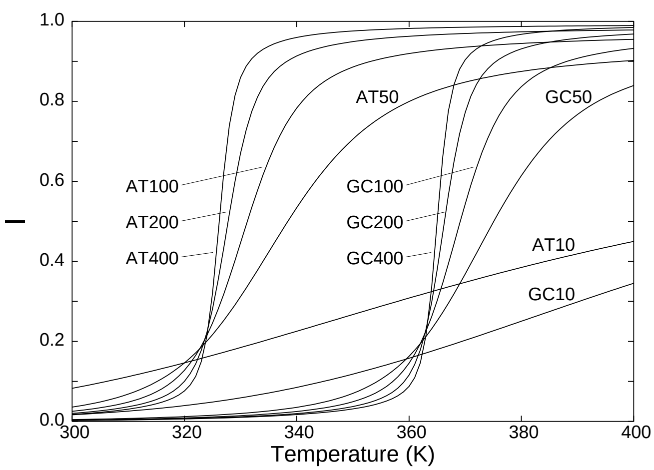

Fig. 1. l (see Eq. (9)) as function of temperature for homogeneous AT and GC chains of different lengths. One can clearly see that, when the length increases, the cur ves resemble more and more a sharp step function. For all sequences free boundary conditions were applied.

integration method of Sec. 5, but could as well been obtained using MD with the bias potential (7). The denaturation curves of the 400 GC and 400 AT base-pair sequences resemble already closely the discontinuous step function, that would result from an infinite chain, and allow to estimate the denaturation temperatures quite accurately. In contrast, previous analysis using MD without any bias had much more difficulty to determine the denaturation temperature due to huge variations in the melting region despite the use of very long sequences upto 16384 base-pairs [39].

4 denaturation curves and bubble probability matrices

Using the definitions of [23,24,25] we can call f the fraction of open base-pairs and p the fraction of open molecules. With the use of Eqs. (4) we can give the following mathematical expressions

$$f = \frac{1}{N}\sum_{k=1}^{N}\langle\theta_k\rangle$$
$$p = \left\langle \prod_{k=1}^{N}\theta_k \right\rangle \qquad (8)$$

Moreover, we introduce l [23,24,25] as the fraction of open base-pairs provided that the molecules is in the double stranded state

$$l = \frac{1}{N}\sum_{k=1}^{N}\langle\theta_k\rangle_\mu \,. \qquad (9)$$

Eq. (8,9) obey the relation $l = (f-p)/(1-p)$. The quantity l is sometimes called the average fractional bubble length. However, this is not completely true as more than one bubble may occur simultaneously in the same sequence. For the infinite case, we have $f = l$ and $p = 0$ as explained in Sec. 3. However, we cannot reproduce the experimental $f(T)$ and $p(T)$ curves for finite chains as we have, strictly speaking, $f(T) = p(T) = 1$ at all temperatures in the PBD model. Therefore, we will focus on the behavior of $l(T)$ which can be measured by the quenching technique of Zocchi and co-workers [23,24,25]. Indirectly, $f(T)$ could be obtained from $l(T)$ using the phenomenological approach of Campa and Giansanti [17]. This approach, however, requires two additional parameters that have to be fitted to experiments. Therefore, we believe that the calculation of $l(T)$ gives the most direct comparison with experimental data.

Of course, the experimental UV absorbance signal cannot be literally related to the fraction of open base-pairs as it is not a binary type measurement that detects whether the base is open or closed. Moreover, the theoretical definition of 'open' and 'close' is a bit ambiguous as it depends on the choice of opening threshold ξ. Still, it is known that the UV absorbance changes quite abruptly when bases move out of stack, which validates the θ-like expressions (8) and (9). Moreover, it was found that, at least, the qualitative aspects of the theoretical denaturation curve are not too sensitive to ξ when chosen within a reasonable interval ($\sim$ [1 Å: 2 Å]) . Nevertheless, the theoretical definitions (8) and (9) are, not the only ones

[1] This is a result from Pólya [52] who proved that one- and two-dimensional random walks always return to their origin. In fact, any site will be visited after an infinite number of steps. The probability to return after an infinite number of steps to the origin is associated with the Pólya's number. This number is 1 for one- and two-dimensional systems, but less than one for higher dimensions.

proposed in literature. In Refs. [40,43] another functional form of Eq. (8) was used

$$f' = \frac{1}{N}\sum_{k=1}^{N}\theta\big(\langle y_k\rangle - \xi\big) \quad (10)$$

We believe, however, that Eq. (10) should be considered as imprecise as the UV signal is almost a binary indication of the stacking state of a base pair and, hence, cannot be related to the mean position $\langle y_k\rangle$ of the bases.

Besides denaturation curves, the statistical method introduced in Ref. [3] allows to study bubbles of a given size. The importance to study bubbles of a given size was suggested by Choi *et al.* [1,2] as its signal could be related to S1 nuclease cleavage experiments and possibly could tell more about its biological function than the mean $\langle y_k\rangle$ or the probability of opening $\langle\theta(y_k-\xi)\rangle$. Before giving the definition of, what we call, the bubble probability matrix, we will need to introduce the following auxiliary function:

$$\begin{aligned}\theta_k^{[m]} &\equiv \bar\theta_{k-\frac{m}{2}}\bar\theta_{k+\frac{m}{2}+1}\prod_{k'=k-\frac{m}{2}+1}^{k+\frac{m}{2}}\theta_{k'} \text{ for } m \text{ even}\\ &\equiv \bar\theta_{k-\frac{m+1}{2}}\bar\theta_{k+\frac{m+1}{2}}\prod_{k'=k-\frac{m-1}{2}}^{k+\frac{m-1}{2}}\theta_{k'} \text{ for } m \text{ odd} \quad (11)\end{aligned}$$

which is 1 (0 otherwise) if and only if k is at the center of a bubble that has exactly size m. For even numbers it is a bit arbitrary where to place the center, but we defined it as the base directly to the left of the midpoint of the bubble. The bubble probability matrix $P_{\rm bub}(k,m)$ is, now, defined as the probability to have a bubble of size m centered at base-pair k provided that the molecule is part of the dsDNAE. Hence,

$$P_{\rm bub}(k,m) \equiv \left\langle \theta_k^{[m]}\right\rangle_\mu \quad (12)$$

In principle, $P_{\rm bub}(k,m)$ contains all the information on the bubble statistics in a DNA sequence. Still, it is useful to calculate other quantities as well. From physical and biological perspective, it might be useful to know the ability to participate in bubbles. Therefore, we introduce the $P_{\rm part}(k,m)$ probability which is the probability to participate in a bubble of at least m sites.

$$\begin{aligned}P_{\rm part}(k,m) \equiv & \sum_{m'\geq m}^{\{m':\ \text{even}\}}\ \sum_{k'=k-m'/2}^{k+m'/2-1} P_{\rm bub}(k',m')\\ &+\sum_{m'\geq m}^{\{m':\ \text{odd}\}}\ \sum_{k'=k-(m'-1)/2}^{k+(m'-1)/2} P_{\rm bub}(k',m') \quad (13)\end{aligned}$$

This quantity is less mathematically stringent as it is independent of where you assign the position of the bubble. Note that this quantity is still somewhat different from the projection in Ref. [3] where each bubble is still associated to one base-pair position only. In variance with $P_{\rm bub}(k,1)$, the bubble participation probability $P_{\rm part}(k,1)$ is directly related to the simple opening. Hence, $P_{\rm part}(k,1) = \langle\theta_k\rangle_\mu \neq P_{\rm bub}(k,1)$.

5 The direct numerical integration method

The two quantities $\langle\theta_k\rangle_\mu$ and $\left\langle\theta_k^{[m]}\right\rangle_\mu$ that appear in Eq. (9) and (12) can be expressed using partition function integrals:

$$\begin{aligned}\langle\theta_k\rangle_\mu &= \frac{Z_{\theta_k}-Z_\Pi}{Z-Z_\Pi}\\ \left\langle\theta_k^{[m]}\right\rangle_\mu &= \frac{Z_{\theta_k^{[m]}}}{Z-Z_\Pi},\end{aligned} \quad (14)$$

which are defined by:

$$\begin{aligned}Z &= \int {\rm d}y^N e^{-\beta U(y^N)}\\ Z_{\theta_k} &= \int {\rm d}y^N e^{-\beta U(y^N)}\theta_k\\ Z_{\theta_k^{[m]}} &= \int {\rm d}y^N e^{-\beta U(y^N)}\theta_k^{[m]}\\ Z_\Pi &= \int {\rm d}y^N e^{-\beta U(y^N)}\times\prod_j\theta_j.\end{aligned} \quad (15)$$

In Eq. (14), we used the fact that $(\theta_k)^2=\theta_k$ and $\theta_k\bar\theta_k=0$. Note that Z, Z_{θ_k}, and Z_Π are infinite, but the differences $Z-Z_\Pi$ and $Z_{\theta_k}-Z_\Pi$ are finite and well defined.

Now, as all integrals Z_X are of the factorizable form $Z_X = \int {\rm d}y^N a_X^{(N)}(y_N,y_{N-1})\ldots a_X^{(3)}(y_3,y_2)a_X^{(2)}(y_2,y_1)$ we can use following iterative scheme to determine the Z_X integrals:

$$\begin{aligned}z_X^{(2)}(y_2) &= \int {\rm d}y_1\, a_X^{(2)}(y_2,y_1)\\ z_X^{(3)}(y_3) &= \int {\rm d}y_2\, a_X^{(3)}(y_3,y_2)z_X^{(2)}(y_2)\\ &\ldots\\ z_X^{(N)}(y_N) &= \int {\rm d}y_{N-1}\, a_X^{(N)}(y_N,y_{N-1})z_X^{(N-1)}(y_{N-1})\\ Z_X &= \int {\rm d}y_N\, z_X^{(N)}(y_N).\end{aligned} \quad (16)$$

The calculation of $z_X^{(k)}(y_k)$ for a discrete set of $n_{\rm grid}$ values y_k requires only $n_{\rm grid}^2$ function evaluations whenever $z_X^{(k-1)}$ is known. Hence, a total of $N\cdot n_{\rm grid}^2$ function evaluations are required instead of $n_{\rm grid}^N$ which is a huge improvement.

An alternative technique was introduced in Ref. [41] where the $a_X^{(k)}(y_k,y_{k-1})$ kernels are expanded into a proper basis-sets. After this expansion, the integrals, like in Eqs. (15), turn into simple matrix multiplications which can be evaluated efficiently. It was found that performance of such a method depends strongly of the right choice of basis-set functions. The implementation of this method is, therefore, probably a bit more involved than the direct integration scheme of Eq. (16). Most likely, this method will be more efficient to calculate quantities as $\langle y_k \rangle$ that are written as averages of continuous functions, than, for instance, $\langle \theta_k \rangle$ which involves a discontinuous step-function. The latter would require a much larger expansion when using continuous basis-set functions.

The factorization of Z_X into $a_X^{(k)}$ kernels is generally not unique. Our choice for $a^{(k)}$ for the partition function Z is the following

$$a^{(k)}(y_k, y_{k-1}) = \begin{cases} e^{-\beta[W(y_k,y_{k-1})+V_{k-1}(y_{k-1})]} & \text{if } k \neq N \\ e^{-\beta[W(y_k,y_{k-1})+V_{k-1}(y_{k-1})+V_N(y_k)]} & \text{if } k = N \end{cases} \quad (17)$$

and for $a_{\Pi}^{(k)}$ and $a_{\theta_q}^{(k)}$

$$a_{\Pi}^{(k)}(y_k, y_{k-1}) = a^{(k)}(y_k, y_{k-1})\theta_k(y_k)\theta_{k-1}(y_{k-1}) \quad (18)$$

$$a_{\theta_q}^{(k)}(y_k, y_{k-1}) = \begin{cases} a^{(k)}(y_k, y_{k-1}) & \text{if } k \neq q, q+1 \\ a^{(k)}(y_k, y_{k-1})\theta_k(y_k) & \text{if } k = q \\ a^{(k)}(y_k, y_{k-1})\theta_{k-1}(y_{k-1}) & \text{if } k = q+1 \end{cases}$$

where we use again that $\theta_k^2 = \theta_k$. Similar expressions can be derived for $a_{\theta_q^{[m]}}^{(k)}$.

In order to perform the numerical calculation, we need to define some proper cut-offs where we can stop the integration. It is natural to stop the integration whenever the weight of a certain configuration $\varrho = e^{-\beta U(y^N)}$ drops below a certain threshold value ϵ. It is clear that the energy diverges and, hence, ϱ vanishes whenever for a certain k the position y_k takes a very large negative value or when the relative distance $|y_k - y_{k-1}|$ becomes very large. To be in safe limits, we calculate the integration cut-offs for the pure AT-chain. If we set the integration boundaries such that outside this domain we have $\varrho < \epsilon$ for this sequence, it will also hold for the pure GC or heterogeneous chain. The lower limit L of y_k results from

$$e^{-\beta V_w(L)} < \epsilon \Rightarrow L \lesssim -\frac{1}{a_w} \ln\Big[\sqrt{\frac{|\ln\epsilon|}{\beta D_w}} + 1\Big] \quad (19)$$

To define the maximal distance d between two neighbors we assume that $\rho e^{-\alpha(y_k+y_{k-1})}$ is almost zero. This yields

$$e^{-\beta\frac{1}{2}Kd^2} < \epsilon \Rightarrow d \gtrsim \sqrt{\frac{2|\ln\epsilon|}{\beta K}}. \quad (20)$$

If $|y_k - y_{k-1}|$ exceeds the value d at any k, the probability distribution $\varrho(y^N)$ must have decreased below the threshold ϵ so that we can stop the integration. The upper limit R is obtained as follows. Again neglecting the anharmonic ρ-term, the configuration with the lowest stacking energy $\sum W(y_k, y_{k-1})$ and with a maximal total stretch $|y_N - y_1| = S$ is obtained whenever equidistant positions are taken such that $|y_k - y_{k-1}| = S/(n-1)$. Then, the total stacking energy equals $(N-1)\frac{1}{2}K(S/(N-1))^2 = \frac{1}{2}KS^2/(N-1) < \frac{1}{2}KS^2/N$. Therefore, the maximum displacement of each base, for configurations that belong to a double stranded configuration, and with $\varrho(y^N) > \epsilon$, cannot exceed R given by

$$R \gtrsim \xi + S \text{ with } S \text{ defined by } e^{-\beta\frac{1}{2}KS^2/N} = \epsilon$$
$$\Rightarrow R \gtrsim \xi + \sqrt{N}d. \quad (21)$$

This completes the set of cut-off values. In principle, the cut-off d is not strictly necessary as L and R are sufficient to start a numerical approach. However, the cut-off d is useful as it decreases the computational expense considerably. To summarize, via Eq. (19-21) we have defined three cut-off values which restrict the configuration space to $L \leq y_k \leq R$ and $|y_k - y_{k-1}| \leq d$ for all k. Any configuration outside this domain must have a Boltzmann weight ϱ below ϵ and can, hence, be neglected for the numerical integration.

The integration boundaries increase only slightly upon decreasing ϵ. Therefore, we took $\epsilon = 10^{-40}$ which is much smaller than actually needed for our required accuracy [3]. As we take a discrete grid with spacing Δy, the values d, L, and R must be adjusted to this grid. That is, we require that $I_d \equiv d/\Delta y$, $I_L \equiv (\xi - L)/\Delta y$ and $I_R \equiv (R - \xi)/\Delta y$ should all be integer values. There is another restriction for the allowed values of I_R which depends on the specific numerical integration method and will be discussed in Appendix A. Coming back to Eqs. (15), we actually no longer intend to calculate Z, Z_{θ_k}, and Z_{Π}, which are infinite, but $Z(R)$, $Z_{\theta_k}(R)$, and $Z_{\Pi}(R)$ which have a linear dependence as function of R. However, the differences $Z(R) - Z_{\Pi}(R)$ $Z_{\theta_k}(R) - Z_{\Pi}(R)$ converge very rapidly to a constant value for $R \to \infty$.

As the same function evaluations are repeated over and over again in this integration scheme (16), it is efficient to store following values at the start of the algorithm using two matrices $M^{(w)}$ and $M^{(s)}$ defined as:

$$M_{ij}^{(w/s)} \equiv \exp(-\beta W(L + i\Delta y, L + (i+j)\Delta y))$$
$$\times \exp(-\beta[V_{w/s}(L + (i+j)\Delta y)]) \quad (22)$$

which are basically the values of two possible $a^{(k)}(y_k, y_{k-1})$ functions (17) on the grid. Then, by defining the vector

$$\chi_X^{(k)}(i) \equiv z_X^{(k)}(L + i\Delta y), \quad (23)$$

the basic operation in Eq. (16)

$$z_X^{(k)}(y_k) = \int \mathrm{d}y_{k-1}\, a_X^{(k)}(y_k, y_{k-1}) z_X^{(k-1)}(y_{k-1})$$

can be recast in following numerical operation

$$\chi_X^{(k)}(i) = \Delta y \sum_j f_j M_{ij}^{(k-1)} \chi_X^{(k-1)}(i+j) \quad (24)$$

where $M_{ij}^{(k-1)}$ is either $M_{ij}^{(w)}$ or $M_{ij}^{(s)}$ of Eq. (22) depending on the type of base-pair $k-1$. Of course, like the end kernel $a^{(N)}(y_N, y_{N-1})$ in Eq. (17), the last matrix in

Eq. (24) should include the additional factor $\exp(-\beta V_N(y_N))$. The vector f_j depends on the specific Newton-Cotes integration method. An analyses of different Newton-Cotes schemes is given in Appendix A.

The algorithm starts by taking the first vector $\chi_X^{(1)}(i) = 1$ and, then, iteratively apply Eq. (24). In order to obtain the full vector $\chi_X^{(k)}(i)$, we need to perform a loop where i runs either from 0 till I_L , from I_L till I_R, or from 0 till $I_L + I_R$ depending on whether X allows y_k in Eq. (16) to take values over the closed, open, or full domain, respectively. At each i, we perform an inner loop over j. Also y_{k-1} might take values in the closed, open or full domain and its value is assigned by the integer $i+j$. Hence, similar to i we can write that $g \leq i+j \leq h$ where g can be either 0 or I_L and h is either I_L or $I_L + I_R$. As $j \sim |y_k - y_{k-1}|$ is also restricted by $|j| \leq I_d$, the inner loop over j runs from MAX$[-I_d, g-i]$ till MIN$[I_d, h-i]$. After the double loop over i and j, we increase k by one and repeat the procedure. This basically defines the complete numerical algorithm, but still leaves open what one should take for the vector f_j. This is discussed in Appendix A in which we consider different integration schemes.

6 bubble probability matrices

Now we have introduced the mathematical definitions concerning the bubble statistics in Sec. 4 and derived the numerical method to calculate these properties in Sec. 5 and Appendix A, we will apply this method to specific sequences. In Ref. [3], we calculated the bubble probability matrix (12) for de adeno-associated viral P5 promoter (AAVP5) whose sequence is shown below

AAVP5: 5'- GTGGCCATTTAGGGTATATATGGCCG
AGTGAGCGAGCAGGATCTCCATTTTG
ACCGCGAAATTTGAACG-3'.

The TSS is shown by an underscore.

In Fig. 2, we show the same results as Ref. [3] for a slightly different threshold value ($\xi = 1$ Å instead of 1.5 Å) together with the bubble partition matrix (13). As we are not interested in the boundary effects, we replicated the chain at both ends, but only computed the statistics for the middle chain. This eliminates the effects of the free ends, which, otherwise, would yield very large opening probabilities at boundary sites [3]. We calculated the bubble probability matrix (12) up to bubbles of size $m = 50$ (only up to 30 is shown in Fig. 2) and the bubble partition matrix from Eq. (13). Note that, for reasons of visualization, we have applied for each row a normalization approach in these two figures. The normalizing constants, which are the maxima in each row, are depicted in the panels below. Considering these results, one can see that the probability for bubbles is approximately exponentially decreasing as function of the bubble size. The bubbles of size ten have probabilities of the order of $\sim 10^{-4}$. This explains the difficulties of previous MD results [1] as the detection of such a large bubble is a true rare event

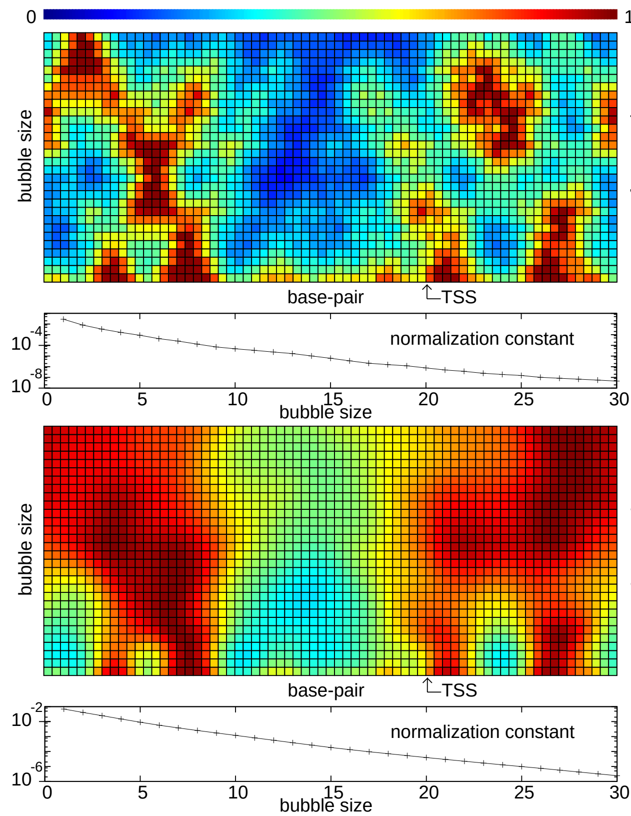

Fig. 2. (Color online) Bubble statistics matrices for the AAVP5 promoter sequen ce for $T = 300K$ and openings threshold $\xi = 1$ Å. Top two panels show the bu bble matrix $P_{\rm bub}(k,m)$ of Eq. (12) and the lower two panels show the bub ble partition matrices $P_{\rm part}(k,m)$ of Eq. (13). Each row m of the first and thir d panel is normalized by the maximum value of the matrix at the given bubble siz e m. The normalization constants as function of m is depicted in the panels below.

on the time-scale accessible by MD. On the other hand, the numerical integration method allows to obtain accurate results for even much larger bubbles. This can be important for the study of biological phenomena as, for instance, transcription elongation involves DNA openings that are larger than ten bases [44]. The method allows to obtain accuracies of less than one percent error after only a few hours of computation which would otherwise take 200 years when using MD [3].

Although Fig. 2 shows indeed somewhat enhanced opening in the biologically active regions, it shows that it is certainly not true that the TSS has a much higher opening probability than the other sites as was found in the foregoing less accurate MD results [1]. In fact, the -30 region shows equal probabilities for opening and and even higher probabilities when bubbles of size ~ 10 are considered. Inspection of the lowest rows in Fig. 2 basically reflects the AT-rich parts of the sequence. The position of the preferential opening for the larger bubbles can be reasonably understood as a merging effect; two small bubbles that are close in distance act as the precursor of a larger bubble whose center is in the middle of the two smaller ones. The $P_{\rm part}$ matrix has considerable less structure, but shows the same tendency.

To investigate whether promoter sites are special in terms of its bubble probability profile, in Refs. [1,3] a human coding gene, known to be free of any protein interaction sites, was examined. The initial results suggested that this sequence had much lower probability for bubbles[1], but the direct integration method showed that the ability for bubble formation was certainly comparable in magnitude to the promoter sequences [3]. Here, we study two other artificial non-promoter sequences. These are the following two complementary Fibonacci sequences:

Fibonacci-1: ACAACACAACAACACAACACAACAA
CACAACAACACAACACAACAACACA
ACACAACAACACAACAACACAACAC
AACAACACAACAAC

and

Fibonacci-2: CACCACACCACCACACCACACCACC
ACACCACCACACCACACCACCACAC
CACACCACCACACCACCACACCACA
CCACCACACCACCA

which have a total length of 89 and a AT content of 62 % and 38 % respectively. The choice for Fibonacci has been made to analyze the hypothetical enhanced opening of biological sequences in comparison with a "random" sequence. However, as a typical random sequence is poorly defined, one could come up with any sequence and basically "prove" what one wants. Therefore we studied the Fibonacci sequences rather than two sequences produced by a random number generator. Although those Fibonacci sequences are far from random, they are sufficiently disordered and have the advantage that they doe not contain very long weak or strong regions due consecutive repetitions. In addition, we strictly rule out that the possibility we pick by accident a sequence that is biologically active as well.

In fig. 3, we show the results of $P_{\rm part}(k,1)$, $P_{\rm part}(k,5)$, $P_{\rm part}(k,10)$ and $P_{\rm part}(k,15)$ for the Fibonacci sequences together with the results for the AAVP5 promoter. The first panel shows $P_{\rm part}(k,1)$ which equals the simple opening probability of the individual base in the sequences. It shows that the promoter sequence has some regions that have a considerably higher affinity to open up than the Fibonacci sequences. This is a result of the presence of longer consecutive AT regions in the AAVP5 promoter. The Fibonacci-1 and Fibonacci-2 sequence have at most 2 or 1 consecutive weak base-pairs in a row. When we examine larger bubbles, we see that the base-specific order of the sequences becomes less important. The extend of the bubble averages out the effect of the precise order of the weak and strong bases. Hence, the openings probability profile becomes more and more determined by the AT content. This is clearly illustrated by the fact that the promoter sequence's probability profile for bubbles of size 15 remains strictly within the two profiles of the Fibonacci sequences at all sites. Hence, the chance to find a bubble of 15 is at each location higher in the AT-rich Fibonacci sequence than in the AAVP5 promoter, despite the absence of long series with consecutive weak AT bases. This also suggest that the bubble statistics, at least within the PBD framework, is reasonably predictable by some simple rules based on the AT content. Indeed, Rapti *et al.* [45,46] suggest that these PBD bubble profiles could be qualitatively reproduced by counting the number of AT-bases within a certain window that is a bit larger than the bubble size considered. Actual DNA in solution seems to be less predictable on basis of the AT content alone. The denaturation steps in long heterogeneous DNA polymers are very sensitive to the sequence [5] and can qualitatively change when only one base-pair is changed. The experimental part of Ref. [1] also suggest that actual DNA bubble statistics retains strong non-local effects. A prerequisite for the understanding of these result would require a more precise interpretation of the measurements by the S1 nuclease cleavage technique expressed in microscopic terms. The experimental signal might well be related to some of the definitions (12) and (13), but probably not straightforwardly. Many questions remain such as which range of bubbles can be detected by S1 nuclease cleavage, where in the bubble takes the cleavage place, is bubble life-time important, and many more. Much more systematic studies are needed. The results of Fig. 3 show that the study of artificial sequences, such as the Fibonacci sequences, can reveal different structures depending on the size of bubbles that are detected. Hence, experimental measurements on artificial periodic and quasiperiodic sequences might be very useful to give some answers to these intriguing questions.

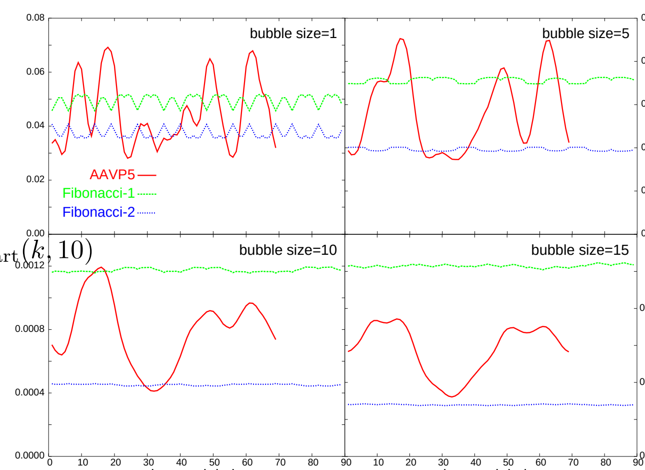

Fig. 3. (Color online) Bubble statistics, $P_{\rm part}(k,1), P_{\rm part}(k,5), P_{\rm part}(k,10)$ and $P_{\rm part}(k,15)$, of the AAVP5 promoter and the Fibonacci sequences.

To summarize this section, our results on the bubble statistics using the accurate direct integration method do not indicate that biologically active sites have a stronger thermally induced enhanced opening than one would expect based on the AT content of the sequences. We also examined the effect of higher temperatures upto 350 K and different openings thresholds upto $\xi = 2$ Å. However, the results remained qualitatively the same. Of course, this does not necessarily mean that there is not such a relation as this would first require a validation of the model. Therefore, in the next section, we will study the theoretical results of the l-denaturation curves that can give a more direct comparison with experimental data than the bubble statistics (12) and (13).

7 Denaturation curves

As explained in Sec. 3, the denaturation curves $f(T)$ and $p(T)$ of Eq. (8) cannot be determined within the PBD framework. Luckily, the $l(T)$ denaturation curve can be calculated using the PBD model and can be measured as well using a recently introduced experimental technique [23,25,24]. For several sequences, Montrichok *et al.* [23,25,24] reported some anomalous behavior of l as function of T. These experimental results are, hence, an excellent benchmark to test the validity of the PBD model. In this section, we show the calculated $l(T)$ curves for the L60B36, L42B18, L33B9, and L48AS given by

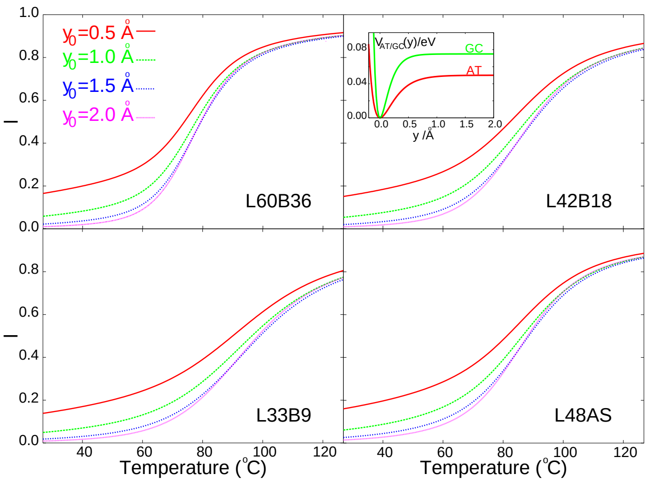

Fig. 4. l versus temperature for 4 heterogeneous sequences L60B36, L42B18, L33B9, and L48AS using four different opening threshold definitions $\xi = 0.5, 1, 1.5$, and 2 Å. Previous MD results of Ares *et al.* [40] were obtained using $\xi = 0.5$ and the different definition of opening Eq. (10). The inset in the right upper panel shows the Morse potential V_k of Eq. (2) for the weak and strong base-pair interaction.

L60B36: CCGCCAGCGGCGTTATTACATTTAA
TTCTTAAGTATTATAAGTAATATGGC
CGCTGCGCC

L42B18: CCGCCAGCGGCGTTAATACTTAAGT
ATTATGGCCGCTGCGCC

L33B9: CCGCCAGCGGCCTTTACTAAAGGCC
GCTGCGCC

L48AS: CATAATACTTTATATTTAATTGGCG
GCGCACGGGACCCGTGCGCCCGCC

In Fig. 4, we show the calculated results for these sequence using four values of ξ: $0.5, 1.0, 1.5$ and 2.0 Å. It is important to note that the different opening threshold values considered do not change the qualitative behavior of the curves. The curves with $\xi = 2$ Å intersect the lower threshold value curves $\xi = 1$ Å and $\xi = 1.5$ Å. This might seem impossible as each base k, that is counted as open because $y_k > \xi = 2$ Å, must also be open when a lower opening threshold value is considered. However, we should bear in mind that ξ not only determines the definition of 'open' and 'closed', but also determines the ensemble via Eqs. (5,6). Considering Eq. (14), it is certainly true that $Z_{\theta_k}(R)$ is strictly decreasing as function of ξ. However, $Z_\pi(R)$ is strictly decreasing as well and, hence, the ratio $[Z_{\theta_k}(R) - Z_{\theta_k}(R)]/[Z(R) - Z_{\theta_k}(R)]$ can actually increase as function of ξ.

The experimental results for the L60B36 and L42B18 sequences contained a remarkable change of slope [23,25,24]. This effect could indicate that the melting appears in two steps in which first an AT rich part of the sequence opens up and is then followed by a GC rich region in the sequence. Our results do not show this signature. This is in contrast with another computational study by Ares *et al.* [40] which does report some of the experimentally found characteristics. However, the change of slope that they found was negative for the both sequences L60B36 and L42B18, while the experimental results showed a very sharp positive change of slope in the L42B18 sequence at a temperature of 70 ℃. Still, the results of Ares *et al.*, for the same sequences we studied, seem to resemble more closely the experimental results than the ones by us. This variance is explained by the following three reasons: (i) Ares *et al.* used the alternative definition of 'open states' as expressed by Eq. (10) instead of Eqs. [8,9]. (ii) They applied a selective use of boundary conditions which were periodic boundary conditions for the sequences L60B36, L42B18, L33B9 and free boundaries, as in this work, for the sequence L48AS. (iii) Ref. [40] allowed for complete denaturation as it was based on a series of short MC simulations without the use of a bias-potential as in Eq. (7). In fact, the work [40] even report on the f and p curves, which cannot unambiguously be determined as we pointed out in Sec. 3. Hence, the deviation from the experimental results must imply that the present PBD model is insufficient to reproduce these non-trivial sequence specific order effects.

However, the experimental results themselves raise some questions. If we were allowed to neglect the DNA-DNA interaction, the $l(T)$ curve seems to provide a signature that is theoretically independent to the concentration of DNA. This is exactly why $l(T)$ can be determined within the PBD framework. Still, it would be interesting to verify experimentally whether the $l(T)$ curve is indeed insensitive to this concentration. Moreover, some of the experimental results are a bit puzzling. The experimental $f(T)$ and $p(T)$ denaturation curves of the L33B9 sequence, for instance, coincide at 75 ℃ while still $f(75\ ℃) = p(75\ ℃) < 1$ [24]. As $l = (f - p)/(1 - p)$, this would imply that $l(T) = 0$ for $T > 75$ ℃. This finding seems to be unphysical and this is probably also the reason that Montrichok *et al.* have depicted the $l(T)$ curve until $T = 75$ ℃ in Ref. [24]. This indicates that one has to be careful when translating the UV absorbance experiments in microscopic terms using Eqs. (8,9). The theoretical development in this field would benefit significantly if more experimental data based on the quenching technique were available.

8 Conclusions

The statistics of thermally induced DNA bubbles has become an important subject of theoretical and experimental studies. Besides the fact that it is a interesting subject from a purely statistical physics point of view, the relation between thermally induced bubbles and biologically active sites has been subject of recent debate. Mesoscopic models, like the PBD model, are a prerequisite in these studies as the experimental data can usually only give indirect information. However, even if a good theoretical model is developed, it is not easy to obtain accurate results as large bubbles occur only seldom in a microscopic system. In previous publications, the inaccuracy inherent to MD have lead to premature conclusions such that the TSS has a much stronger affinity to form bubbles than any other arbitrary site [1,2]. In a recent publication by us [3], we showed, using a new statistical method that is orders of magnitude faster than MD, that this statement had to be reconsidered. Although the biologically active sites have some enhanced opening due to their relative high content of weak AT base-pairs, the bubble probability profile given by the PBD model was certainly not sufficient to make accurate predictions on transcription sites or to discriminate between biologically active and inactive sequences. Hence, this implies that either the biologically active sites cannot be assigned by the information of thermally induced bubbles alone or the actual PBD model is insufficient to describe all the sequence specific effects correctly. The S1 nuclease experiments seem to suggest a correlation between bubbles *in vitro* and transcription sites. It is, however, not exactly clear how the S1 nuclease measurements should be translated in microscopic terms that can be calculated by computer experiments.

In this article, we have revisited the direct numerical integration technique that was introduced in [3]. We have given a detailed explanation of the algorithm and investigated the performance of different integration schemes. Although the higher order Newton-Cotes schemes are better for very high precision results with many digits, the simple Simpson $\frac{1}{3}$-rule or Boole's rule are more efficient if only an accuracy of a few percent is required. The optimal result is obtained when the Simpson's or Boole's rule is combined with the simple rectangular rule. The latter is used when the function vanishes at the two integration boundaries. Moreover, we have given a thorough discussion on how to treat finite chains using the PBD model by introducing the double stranded DNA ensemble. This eliminates all the problems due to the unnormalizability of equilibrium distribution in the full space and gives results that can be compared by experiments performed below the melting temperature.

Within this ensemble, we have defined two types of bubble probabilities. $P_{\rm bub}(k, m)$ is the probability that a bubble of exactly size m is centered at base-pair k. $P_{\rm part}(k, m)$ is the participation probability that site k is inside a bubble of at least m bases long. Our analyses on the AAVP5 promoter sequence and two artificial Fibonacci sequences confirm what we found before [3]. No theoretical evidence was found that bubbles appear more frequently at transcription sites than at other sites that have a similar AT content. When larger bubbles are considered, the effect of sequence specific order becomes even less important. A recent theoretical study of Rapti *et al.* [45] confirms this and reveals that the PBD bubble statistics profile can be qualitatively reproduced by counting the number of AT within a certain window that is larger than the bubble size. The questions remains whether this is also true for actual DNA. The S1 nuclease experiments suggest that the behavior of real DNA is more complicated than that.

To study the validity of the PBD model, we applied our method to calculate the so-called l-denaturation curves that allow to make a more direct comparison to experimental results. As argued, the standard f-denaturation curve cannot be obtained without additional parameters due the problem of normalizability for finite DNA chains. Luckily, the l-denaturation curves can be measured as well via a recently introduced quenching technique [23,24,25]. Our theoretical calculations did not reproduce the experimentally found anomalies of the $l(T)$ denaturation curve. This points out a significant weakness of the present PBD model. This also implies that the bubble hypothesis postulated by Choi *et al.* [1] could still be supported by theoretical evidence whenever an 'ideal' DNA model is considered. The indirect evidence of the S1 nuclease experiments is yet insufficient to make this statement absolute as its meaning in terms of microscopic terms is not yet completely understood. It is also difficult to believe that the statement holds for all TSS as some transcription sites are known that consists of at least three consecutive strong base in a row [47]. More systematic experimental and theoretical studies are required.

Theoretical improvement can probably be achieved when a more complicated stacking interaction is taken into account. We found that some of the anomalies found by Montrichok *et al.* [23,24,25] could be reproduced using a different base-pair specific stacking potential $W(y_k, y_{-1})$ (2) [48]. However, more complicated potentials might be needed. It is important to note that the direct integration method is not restricted to the PBD model only. It can be used whenever the proper factorization (16) can be applied. Our preliminary results indicate that the PBD model could be improved considerably while still maintaining the one-dimensional character of the model. This implies that the direct integration method could still be applied for this new class of models and will, hence, probably remain an important method for the future theoretical developments in this field.

We would like to thank Johannes-Geert Hagmann for useful discussions and critically reading this manuscript. TSvE has been supported by a Marie Curie Intra-European Fellowships (MEIF-T-2003-501976) within the 6th European Community Framework Programme and by the Belgium IAP-network. SCL has been supported by the Spanish Ministry of Science and Education (FPU-AP2002-3492), project BFM 2002-00113 DGES and DGA (Spain) and by the CAI-Europa XXI program.

A Newton-Cotes integration schemes

In Sec.5, we have given the derivation of the direct integration method upto the numerical implementation which basically comprises an iterative operation of Eq. (24). The vector f_j depends on choice of Newton-Cotes integration scheme. In general, the Newton-Cotes numerical integration approximates any integral over an finite range $\int_a^b g(x)\,\mathrm{d}x$ by $\Delta y \sum_{i=0}^n f_i\, g(a+i\Delta y)$ with $n=(b-a)/\Delta y$. From the various Newton-Cotes schemes, we will discuss the simple rectangular rule, Simpson $\frac{1}{3}$-rule, Boole's rule, and the 11-point Newton-Cotes formula. The corresponding f_i vectors are listed below.

Rectangular rule:

$$f_i = 1 \text{ for all } i, \tag{25}$$

Trapezoidal rule:

$$f_i = \begin{cases} \frac{1}{2} & \text{for } i=0,n \\ 1 & \text{for } i=1,2,3,\ldots,n-1 \end{cases}, \tag{26}$$

Simpson's $\frac{1}{3}$ rule:

$$f_i = \frac{1}{3} \times \begin{cases} 1 & \text{for } i=0,n \\ 4 & \text{for } i=1,3,5,\ldots,n-1 \\ 2 & \text{for } i=2,4,6,\ldots,n-2 \end{cases}, \tag{27}$$

Boole's rule [49]:

$$f_i = \frac{2}{45} \times \begin{cases} 7 & \text{for } i=0,n \\ 32 & \text{for } i=1,5,9,\ldots,n-1 \\ 12 & \text{for } i=2,6,10,\ldots,n-2 \\ 32 & \text{for } i=3,7,11,\ldots,n-3 \\ 14 & \text{for } i=4,8,12,\ldots,n-4 \end{cases}, \tag{28}$$

and the 11-point Newton-Cotes rule [50]:

$$f_i = \frac{5}{299376} \times \begin{cases} 16067 & \text{for } i=0,n \\ 106300 & \text{for } i=1,11,21,\ldots,n-1 \\ -48525 & \text{for } i=2,12,22,\ldots,n-2 \\ 272400 & \text{for } i=3,13,23,\ldots,n-3 \\ -260550 & \text{for } i=4,14,24,\ldots,n-4 \\ 427368 & \text{for } i=5,15,25,\ldots,n-5 \\ -260550 & \text{for } i=6,16,26,\ldots,n-6 \\ 272400 & \text{for } i=7,17,27,\ldots,n-7 \\ -48525 & \text{for } i=8,18,28,\ldots,n-8 \\ 106300 & \text{for } i=9,19,29,\ldots,n-9 \\ 32134 & \text{for } i=10,20,30,\ldots,n-10 \end{cases} \tag{29}$$

The right choice of integration scheme can significantly improve the precision of the method. One cannot say in advance that the highest order scheme is always preferable. This can depend on the shape of the function g, the applied integration boundaries, and the required precision. In order to study the accuracy of the integration methods, we applied the different schemes (25-29) on the standard integral $\int_a^\infty e^{-x^2}\,\mathrm{d}x$ where we take $a=-\infty, 0$ and 1. We take a numerical cut-off such that $|x| \leq 10$ on the integration domain. In general, the higher order Newton-Cotes numerical integration schemes require that the total number of integration intervals n must be multiples of a certain value. These are 2, 4, and 10 for, respectively, Simpson's rule, Boole's rule and 11-point Newton-Cotes. However, as the function vanishes at the right boundary ($x=10$ in our numerical approach) we can take the semi-infinite analogue where we start with f_0 at the point $x=a$ (or $x=-10$ if $a=-\infty$) and then simply continue with $f_1, f_2, \ldots$ until the point $x=10$ without requiring the correct ending $f_n = f_0$.

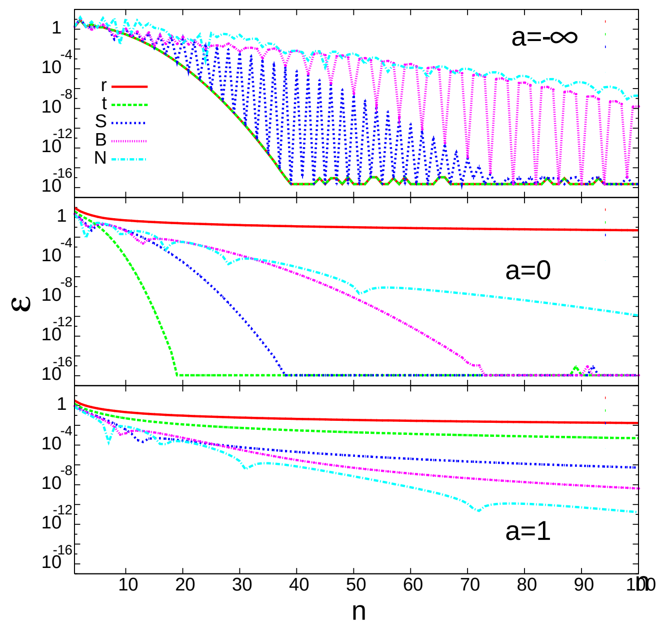

Fig. 5. (color online) The absolute error for the integration of $\int_a^\infty \exp(-x^2)\,\mathrm{d}x$ as function of the number of intervals n in the numerical approach. The rectangular rule (r), trapezoidal rule (t), Simpson's $\frac{1}{3}$-rule (S), Boole's rule (B), and the 11 point Newton-Cotes scheme (N) are compared. Three cases are considered: $a=-\infty$ (top), $a=0$ (middle), and $a=1$ (bottom). The horizontal plateau in the first two panels is a result from the cut-off at ± 10.

In fig. 5, we have plotted the integration errors as function of n obtained by the five Newton-Cotes methods and the three values of a. We see that the highest order scheme is not always the best choice. In fact, for the integration over the full range ($a=-\infty$), the simple rectangular rule is identical to the trapezoidal rule, but far superior to the other methods (27-29). Naturally, as the function vanishes at both ends, the result would not change much upon shifting the initial point to $-10 + \Delta x$. Averaging over several shifts using Eqs. (27-29) results in a weighted summation that approaches the simple rectangular rule (25). The optimum performance of the rectangular rule on the infinite domain is, hence, not surprising.

The trapezoidal rule gives the optimal result for the case $a = 0$. Also this is not too surprising as the function is symmetric and the trapezoidal rule is exactly half the result of the rectangular rule over the full domain. For $a = 1$ we find, as expected, that the 11-point Newton-Cotes method gives the best result. However, only at large n the difference becomes apparent.

We also analyzed the performance of the different Newton-Cotes schemes for the bubble statistics in the PBD model. As a benchmark, we compared the calculated values of l (9) at temperature $T = 300$ K and threshold opening $\xi = 1$ Å for a 10 base-pair long homogeneous AT chain with free boundaries. Considering previous results, we always applied the rectangular rule for the integrals in (16) when the integrated function vanishes at both integration or cut-off boundaries in y_{k-1}. These are either at $y_{k-1} = L$ or at $y_{k-1} = y_k \pm d$. When the integrated function only vanishes at one end, we applied the semi-infinite variation of one of the Newton-Cotes formulas [25-29]. It is important to notice that, as we mentioned before, the distribution function is not vanishing at $y_{k-1} = R$. Hence, the Newton-Cotes rule needs to be applied at this boundary for an optimal accuracy; i. e. we start with f_0 at this boundary and continue in the negative direction $R - \Delta y, R - 2\Delta y, \ldots$ for the numerical integration.

The integrals with two non-vanishing boundaries appear only for the last integrations $Z_X = \int \mathrm{d}y_N Z_X^{(N)}$ in Eq. (16) and when y_N must be integrated over the open domain only. Then, both at the left boundary $y_N = \xi$ as at the right boundary $y_N = R$, the function is not necessarily decayed below ϵ. This also implies that $R - \xi$ is the only interval that must be a special multiple of Δy. This must be an multiple of 2 for Simpson's rule, 4 for Boole's rule and 10 for 11-point Newton-Cotes rule and this gives the restriction to the possible integer values that I_R can take.

After these technical details are taken into account, the Newton-Cotes formulas [25-29] can be applied to the benchmark system and allow to compare the different integration methods. The results are depicted in table 1. These show that it is certainly beneficial to go beyond the simple rectangular or trapezoidal rule. Although, higher order schemes like the 11-point Newton-Cotes are presumably better at very small values of Δy and very high precision, at larger values of Δy the Simpson's and Boole's method give better results. The highest precision results with $\Delta y = 0.0125$ Å show an accuracy of 8 digests for both Simpson, Boole and 11-point Newton-Cotes, while the computational expense is less than a minute. Such a performance is far beyond any MD or MC method even if enhanced sampling is applied [51].

For our purposes, an accuracy a few percent is enough. Therefore, considering the results of Fig. 5 and Table 1, we have chosen to use Simpson's rule with a grid spacing of $\Delta y = 0.1$. In the results of Sec. 6 and 7, we have always used these parameters.

References

1. C. H. Choi *et al.*, Nucl. Acid Res. **32**, 1584 (2004).
2. G. Kalosakas *et al.*, Eur. Phys. Lett. **68**, 127 (2004).
3. T. S. van Erp, S. Cuesta-López, J.-G. Hagmann, and M. Peyrard, Phys. Rev. Lett. **95**, 218104 (2005).
4. R. B. Inman and R. L. Baldwin, J. Mol. Biol. **8**, 452 (1964).
5. R. M. wartell and A. S. Benight, Phys. Rep. **126**, 67 (1985).
6. U. Dornberger, M. Leijon, and H. Fritzsche, J. Biol. Chem. **274**, 6957 (1999).
7. H. Urabe and Y. Tominaga, Biopolymers **21**, 2477 (1982).
8. L. Movileanu, J. M. Benevides, and G. J. Thomas, Biopolymers **63**, 181 (2002).
9. H. Grimm and A. Rupprecht, in *Nonlinear excitations in biomolecules*, *Les Editions de physique*, edited by M. Peyrard (Springer-Verlag, Berlin, 1995), p. 101.
10. G. Altan-Bonnet, A. Libchaber, and O. Krichevsky, Phys. Rev. Lett. **90**, 138101 (2003).
11. M. Y. Azbel, Phys. Rev. A **20**, 1671 (1979).
12. J. Santa Lucia Jr, Proc. Natl. Acad. Sci. USA **95**, 1460 (1998).
13. D. Poland and H. A. Scheraga, J. Chem. Phys. **45**, 1456 (1966).
14. C. Kittel, Am. J. Phys. **37**, 917 (1969).
15. M. Peyrard and A. R. Bishop, Phys. Rev. Lett. **62**, 2755 (1989).
16. T. Dauxois, M. Peyrard, and A. R. Bishop, Phys. Rev. E **47**, R44 (1993).
17. A. Campa and A. Giansanti, Phys. Rev. E **58**, 3585 (1998).
18. C. J. Benham, Proc. Natl. Acad. Sci. USA **90**, 29995 (1993).
19. C. J. Benham, J. Mol. Biol. **255**, 425 (1996).
20. R. M. Fye and C. J. Benham, Phys. Rev. E **59**, 3408 (1999).
21. C. J. Benham and C.-P. Bi, J. Comput. Biol. **11**, 519 (2004).
22. C.-P. Bi and C. J. Benham, Bioinformatics **20**, 1477 (2004).
23. A. Montrichok, G. Gruner, and G. Zocchi, Eur. Phys. Lett. **62**, 452 (2003).
24. Y. Zheng, A. Montrichok, and G. Zocchi, J. Mol. Biol. **339**, 67 (2004).
25. Y. Zheng, A. Montrichok, and G. Zocchi, Phys. Rev. Lett. **91**, 148101 (2003).
26. M. Peyrard and T. Dauxois, Math. Comp. Sim. **40**, 305 (1996).
27. M. Joyeux and S. Buyukdagli, Phys. Rev. E **72**, 051902 (2005).
28. A. Campa and A. Giansanti, J. Biol. Phys. **24**, 141 (1999).
29. L. A. Marky and K. J. Breslauer, Biopolymers **21**, 2185 (1982).
30. K. J. Breslauer, R. Frank, H. Blocker, and L. A. Marky, Proc. Natl. Acad. Sci. USA **83**, 3746 (1986).
31. J. SantaLucia, H. T. Allawi, and P. A. Seneviratne, Biochemistry **35**, 3555 (1996).
32. R. L. Ornstein, R. Rein, D. L. Breen, and R. D. Macelroy, Biopolymers **17**, 2341 (1978).

33. W. Saenger, *Principles of Nucleic Acid Structure* (Springer-Verlag, Berlin, 1984).
34. P. Mignon, S. Loverix, J. Steyaert, and P. Geerlings, Nucl. Acid Res. **33**, 1779 (2005).
35. P. Hobza and J. Sponer, Chem. Rev **99**, 3247 (1999).
36. J. Sponer, J. Leszczynski, and P. Hobza, Theochem-J. Mol. Struct. **573**, 43 (2001).
37. M. Peyrard, Nonlinearity **17**, R1 (2004).
38. N. Theodorakopoulos and M. Peyrard, Phys. Rev. Lett. **85**, 6 (2000).
39. T. Dauxois, M. Peyrard, and A. R. Bishop, Phys. Rev. E **47**, 684 (1993).
40. S. Ares, N. K. Voulgarakis, K. O. Rasmussen, and A. R. Bishop, Phys. Rev. Lett. **94**, 035504 (2005).
41. Y. l Zhang, W.-M. Zheng, J.-X. Liu, and Y. Z. Chen, Phys. Rev. E **56**, 7100 (1997).
42. R. A. Neher and U. Gerland, Phys. Rev. E **73**, 030902 (2006).
43. S. Buyukdagli, M. Sanrey, and M. Joyeux, Chem. Phys. Lett. **419**, 434 (2006).
44. K. S. Murakami *et al.*, Science **296**, 1285 (2002).
45. Z. Rapti, A. Smerzi, K. O. Rasmussen, and A. R. Bishop, Eur. Phys. Lett. **74**, 540 (2006).
46. Z. Rapti *et al.*, Phys. Rev. E **73**, 051902 (2006).
47. D. J. Galas, M. Eggert, and M. S. Waterman, J. Mol. Biol. **186**, 117 (1985).
48. S. Cuesta-López et al, to be published .
49. G. Boole and J. F. Moulton, *A Treatise on the Calculus of Finite Differences, 2nd rev. ed.* (Dover Publications, New York, 1960).
50. A. M. Abramowitz and I. A. Stegun, *Handbook of Mathematical functions* (Dover Publications, New York, 1972).
51. G. M. Torrie and J. P. Valleau, Chem. Phys. Lett. **28**, 578 (1974).
52. G. Pólya, Math. Ann. **84**, 149 (1921).

Δy	0.2	0.1	0.05	0.025	0.0125
r	1.7059	1.6112	1.57187104	1.5520500628	1.5422425176
t	1.5506	1.5339	1.53313317	1.5326609537	1.5325428897
S	1.5015	1.5307	1.53253332	1.5325035590	1.5325035346
B	1.4887	1.5333	1.53258630	1.5325015790	1.5325035330
N	1.1940	1.5156	1.53183258	1.5325009318	1.5325035341

Table 1. Analysis of the accuracy of the Newton Cotes integration scheme. $l(10^{-1})$ for a 10 base-pair homogeneous AT chain is shown for different values of Δy. 5 integration schemes are compared: rectangular rule (r), trapezoidal rule (t), Simpson's $\frac{1}{3}$-rule (S), Boole's rule (B), and 11-point Newton-Cotes formula (N).